

# Enhanced Information Extraction from Cylindrical Visual-Tactile Sensors via Image Fusion

Zilan Li, Zhibin Zou, Weiliang Xu, Yuanzhi Zhou, *Student Member, IEEE*, Guoyuan Zhou, Xuan Huang, and Xinming Li, *Member, IEEE*

**Abstract**—Vision-based tactile sensors equipped with planar contact structures acquire the shape, force, and motion states of objects in contact. The limited planar contact area presents a challenge in acquiring information about larger target objects. In contrast, vision-based tactile sensors with cylindrical contact structures could extend the contact area by rolling, which can acquire much tactile information that exceeds the sensing projection area in a single contact. However, the tactile data acquired by cylindrical structures does not consistently correspond to the same depth level. Therefore, stitching and analyzing the data in an extended contact area is a challenging problem. In this work, we propose an image fusion method based on cylindrical vision-based tactile sensors. The method takes advantage of the changing characteristics of the contact depth of cylindrical structures, extracts the effective information of different contact depths in the frequency domain, and performs differential fusion for the information characteristics. The results show that in object contact confronting an area larger than single sensing, the images fused with our proposed method have higher information and structural similarity compared with the method of stitching based on motion distance sampling. Meanwhile, it is robust to sampling time. We complement this method with a deep neural network to illustrate its potential for fusing and recognizing object contact information using cylindrical vision-based tactile sensors.

**Index Terms**—cylindrical structure, tactile information fusion, vision-based tactile sensors

## I. INTRODUCTION

Tactile sensing [1]-[5] is significant in various domains, including robotics [6][7], electronic skin [8][9], and human-computer interaction [10][11]. Nowadays, the detection scenarios tend to be more complex and the detection requirements are improving increasingly. As a response to this shift, vision-based tactile sensors [12][13] like GelStereo [14] and TacTip [15] have garnered substantial attention in the realm of texture discrimination, surface analysis, and related research endeavors, owing to their exceptional integration and impressive resolution. The sensing region on the surface of a vision-based tactile sensor produces deformation when it is in

contact with an object. This deformation data encodes the condition of the contacted object into an optical image suitable for archival and analytical purposes. However, the comprehensive acquisition of surface data remains unattainable due to the limited sensing area in large object detection scenarios. Consequently, how to extend the sensing area to handle the detection tasks in large areas is an important issue for contact-type sensors.

At present, extending the sensing area can be resolved by modifying the structure [16]. The surface of the sensor contact structure is designed in a curve [17][18], thus allowing the contact position to change by tilting after contact with the object. In addition, an effective structural design solution is to make the contact module and the imaging module not fixedly connected and movable relative to each other. Then, the curved contact areas are merged and form a cylindrical outer surface. This design permits the sensor to roll in one direction, continuously acquiring data and expanding the contact area. This cylindrical structure of the vision-based tactile sensor was capable of continuously acquiring tactile data during motion for application in inspection tasks [19] [20]. However, due to their non-planar shape, whether cylindrical or generally curved, the acquired tactile information is not at a uniform depth level. The images contain contact states at varying depths. Furthermore, since the focal plane of the camera is generally set at a position tangent to the curves, this resulted in other regions being in an unfocused imaging state. In related studies [21], tiny areas at the center of each image captured in motion, which are assumed to be at the same depth, assemble the scanned regions. This approach requires strict temporal synchronization and does not effectively utilize tactile information for other image regions.

In order to discern and extract the components that represent the object's situation within images containing contact data at varying depths, we present an image fusion method based on cylindrical vision-based tactile sensors. The stitching of actual contact data is realized by fusing tactile information from multiple images. Considering these images encapsulate diverse contact states at varying depths and are distributed across an image sequence, the method extracts the overall features and edge features of the object's contact in the frequency domain. Further, combining the contact depth characteristics of the cylindrical structure, a differentiated fusion calculation is adopted for different features. The method summarizes the information that reflects the actual shape of the contact location in the image and presents it in a single image. Through experiments, we verify that the fused

Manuscript submitted November 7, 2023. This work was supported by the Guangdong Basic and Applied Basic Research Foundation (No. 2022A1515010136), the Guangdong Provincial Key Laboratory of Nanophotonic Functional Materials and Devices, and the South China Normal University start-up fund. (*Corresponding author: Xinming Li*).

Zilan Li, Zhibin Zou, Weiliang Xu, Yuanzhi Zhou, Guoyuan Zhou, Xuan Huang and Xinming Li are with Guangdong Provincial Key Laboratory of Nanophotonic Functional Materials and Devices, School of Information and Optoelectronic Science and Engineering, South China Normal University, Guangzhou 510006, People's Republic of China. (e-mail: xml@scnu.edu.cn)

images obtained using our proposed method have higher information and structural similarity compared to the method of stitching based on motion distance sampling. The proposed method can utilize the tactile data at each depth level in the image to restore the contact information and is robust to sampling time. We demonstrate the effectiveness of the method on everyday objects and defects. Furthermore, when integrated with a deep neural network trained using congruent image sequences, the proposed method has the potential to realize the fusion and detection of contact scenarios simultaneously. This method showcases its potential for various applications, such as product manufacturing and quality inspection.

## II. CONTRIBUTION OF STRUCTURE TO TACTILE IMAGES

### A. Comparison of different structures

The sensor operating scene is shown in Fig. 1(a). Objects along its path are captured in images. The sensor comprises an imaging module, a flexible contact layer, and a supporting structure, as depicted in Fig. 1(b). The flexible contact layer is subject to rolling motion, and the imaging module is continuously focused on the contacting object. Upon contact, the flexible contact layer will deform, causing a change in the variation of the image pattern captured by the camera, revealing the contact in the image. The cylindrical vision-based tactile sensor structure is distinct in its image content compared to planar sensors. A comparison is made to discuss the visibility of this feature. The primary structure of the sensor was crafted using PLA and quartz. We employed PDMS [22], Smooth-On Skin Tite silica gel and TiO<sub>2</sub> powder to create a flexible contact layer equipped with a reflective film. We utilized readily available embedded camera and light source components, including a commercial camera and LED single beads. We prepared vision-based tactile sensors for contrasting planar contact areas using the same materials and processes. The sensor was placed on the test platform employing a force gauge and displacement stage for testing, shown in Fig. 2(a). A 3D-printed matrix probe, composed of 4x3 rectangular structures (1 mm x 1 mm x 2 mm) with 2 mm spacing, was mounted on the force gauge to evaluate deformation characteristics. Deformational characteristics were indicated by measuring the difference in gray values between images taken at sampling locations and images captured when no force was applied. Three equidistant sampling points were chosen on each side of the contact area.

In Fig. 2(b), we observe that the planar structure exhibits uniform deformation across its regions. In contrast, Fig. 2(c) shows that the change in gray value in the middle of the cylindrical structure is significantly higher than the sides. This shows that the cylindrical structure causes the center region to have a greater contact depth for the same force, resulting in greater deformation. The regions on the sides show a gradual response as the force increases. When the sensor contacts an object, some region of the contact layer detects varying levels of deformation due to the hard material. As the sensor rolls, the contact process progresses from edge to center and then

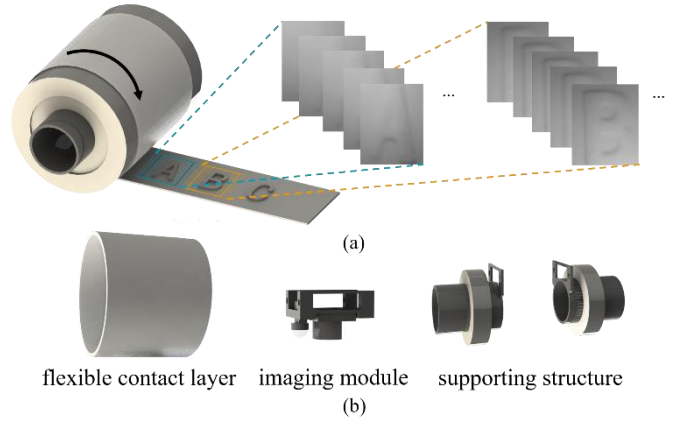


**Fig. 1.** Working schematic and structural components. (a) The sensor follows a defined path for data collection, with the capability to roll smoothly along its trajectory. (b) The sensor's structural components.

back to the edge, effectively capturing contact information at various depths. It starts from a shallow depth, progresses to a deeper level, and then returns to a shallower depth within a localized area. Simultaneously, though the contact surfaces of the probes make the deformations of each position different, their positions in the image correspond with the actual positions, ensuring a faithful representation of relative spatial relationships. Fig. 2(d) illustrates the consistent correlation between contact depth and normal force in both structures, and the difference mainly comes from the difference between the thickness and the force region. The sensory field size of the camera in real space calculated using the contact matrix is demonstrated in Fig. 2(e). Further support can be provided to establish the relationship between the temporal and spatial domains.

### B. Principle Analysis of Structures

The image, which carries the contact information, contains all the data for analysis. They convey the changes produced in the flexible contact layer through optical signals. The geometric configuration of the cylindrical vision-based tactile sensor is visually depicted in Fig. 3(a), where Region I and Region II represent two perpendicular cross-sections. Light is transmitted inside the sensor to the flexible contact layer surface, where it is reflected due to the presence of a reflective layer and captured by the camera. We regard the inner surface of the flexible contact layer as a diffuse reflective surface. By applying Lambert's cosine law [23] to account for reflection, we can derive the expression for the intensity of reflected light. For a point in the image:

$$L_{ij} = F(\alpha_i, \alpha_j, \beta_{ij}) \quad (1)$$

where  $i, j$  denotes the position of the point in the image.  $\alpha_i$  and  $\alpha_j$  are the angles converted from the positions. Each point's actual contact location is uniquely and deterministically mapped within the image.  $\beta_{ij}$  signifies the angle formed between the surface normal of the point's location and the

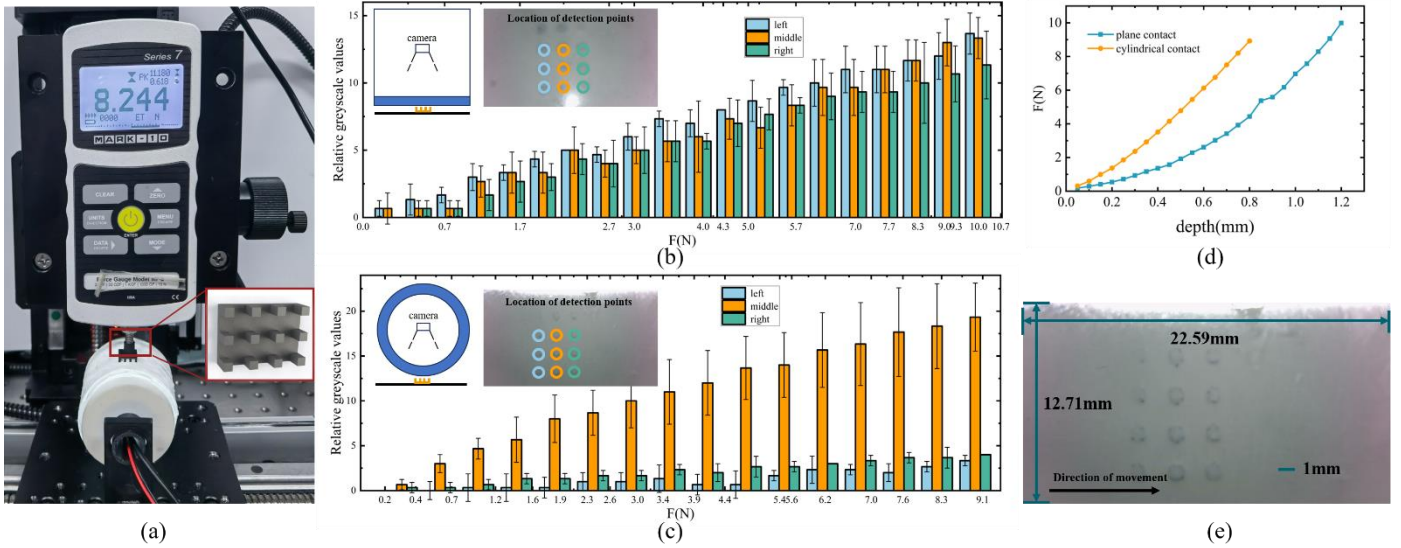


**Fig. 2.** Sensor testing. (a) The scenario of the test. (b)(c) The schematic diagrams of the testing of the planar and cylindrical structures, the location of the sampling point, and the relationship between the magnitude of the normal force and the amount of change in pixel value when pressed at different locations. (d) The relationship between the contact depth and the magnitude of the normal force applied to the cylindrical and planar structures. (e) The scaling relationship of the sensor camera field of view in real space.

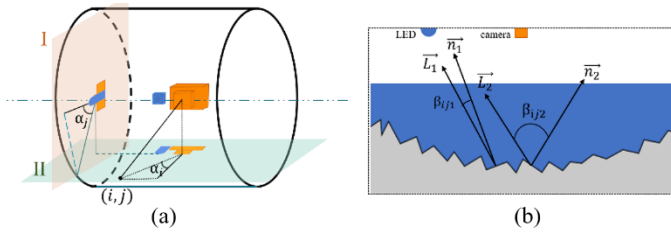


**Fig. 3.** Schematic diagram of the main structure. (a) Simplified schematic of the geometric relationship between the internal imaging system of the sensor and the external structure. Region I and Region II represent two perpendicular cross-sections. (b) Schematic of the change in the geometric relationship of the deformation of the flexible contact layer in contact with an object.

direction of the light source. This angle varies depending on the received contact, as exemplified in Fig. 3(b). The gray value of a point in an image is affected by the location and the deformation of the point on the surface opposite to it. The points on the contact region collectively reflect the contact state of the object and consist to a tactile image. Therefore, the information contained in the image will include deformation positions and variables. The grayscale value assigned to each position within the tactile image faithfully signifies the extent of deformation on the contact surface when all other conditions remain unchanged.

The tactile image also captures the phenomenon of varying contact depths caused by the cylindrical structure. As shown in Fig. 4(a), the deformation induced by an object in contact with the sensor is not uniform for each region of the flexible contact layer due to the cylindrical structure. This results in the acquired tactile images containing deformation data from different contact depths. The information contained therein can represent the state of the object's surface at various depths,

which helps analyze the actual surface condition. As the sensor rolls, different sensor regions come into contact with the object (Fig. 4(b)). The data containing the contact conditions at various depths of the object are stored in a sequence of images. Each tactile image records contact data at various depths within a region, collectively serving as the foundation for image fusion.

### III. FUSION USING IMAGE SEQUENCES

#### A. Algorithm Discussion

The non-planar contact structure of cylindrical vision-based tactile sensors leads to different depths of object contact information in a single image. In general, different contact depths of the sensor's flexible contact layer with an object will cause different degrees of deformation of the flexible material. The deformation is more obvious for deeper contact and is also closer to the shape of the object contacted. This means that the deformation of the deepest contact with an object conveys the object's actual shape. Since the target has a certain projected area, the image sequence containing the target exhibits distributed contact data from these deepest positions after rolling acquisition by the sensor. The task is to extract and fuse the contact data containing the target object. In an image sequence, the whole shape of the object and the edge information are present at different frequencies, which can be used to identify the object's actual shape, so it is important to separate them from the background and the noise. Therefore, Daubechies wavelet transform [24] is used to transform the image data into the frequency domain for processing. The wavelet transform can store the information of different frequencies in different subbands for extraction.

Fig.5(a)(b) illustrates the acquisition process and the original image of an alphabet image sequence. As the sensor

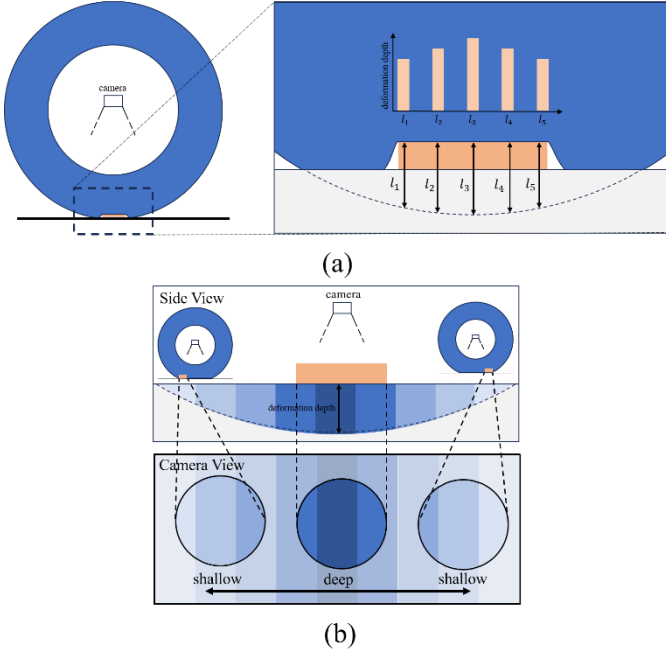


**Fig. 4.** Schematic diagram of contact status. (a) The sensor's flexible contact layer comes into contact with the object, inducing deformations that correlate with the contact position. (b) The contact depth data was collected during contact with the object.

rolls during acquisition, the object shifts position within the image. The template-matching algorithm [25] was employed to delineate the target region to ensure precise alignment. In addition, to better display the message, the binarized image is shown in Fig. 5(c). Three alphabets are focus captured in each of the three images. The transformation was implemented in Python using the Pywalvets library, resulting in four subbands in total. A low-frequency subband captures basic object structure and global features. Three high-frequency subbands, carrying subtle features such as edges and details, are computed in horizontal, vertical, and diagonal directions. Considering the complexity of the texture and the possible presence of features with strong directionality, the three directions are captured in favor of obtaining as many high-frequency features as possible. We adopt different fusion strategies for the subbands. To address noise and maintain structural information, we employed averaging fusion for the low-frequency subbands. The edges and details data carried by the high-frequency portion reflect the local features of the object and represent the shape of the acquired object. We selected the maximum gray scale value at each position. This value represents the peak deformation of the flexible contact layer during contact with the target object. It is typically corresponding to the deepest point of contact with the object. Fig. 6(a) displays the sequential image fusion, resulting in the final fused sub-bands shown in Fig. 6(b). Subsequently, an inverse transformation was applied to generate the fusion result, illustrated in Fig. 6(c).

The fused image takes the actual contact information (clear

alphabets seen in the image), which initially existed in separate images, and fuses them on a single image. This shows that our method realizes the splicing of effective information in the contact process. The acquisition of image sequences can be continuous with uniform pressure application. This means that the number of images to be fused is adjustable and can be adapted to scenes with finer and more complex textures. At the same time, the fusion process is a screening of the contact data at different depths. For objects with substantial depth variations, such as raised defects, capturing their shape at multiple depths enables feature analysis.

## B. Experiment

We validate our method through experiments involving graphic matrices elevated 1 mm from the plane, featuring pattern units such as points, linear lines, and curves, as seen in Fig. 7. The sensor captured and the fusion algorithm processed the image sequence. We selected different numbers of images in the image sequence for fusion, and the splicing performed using the method of stitching based on motion distance sampling was used for contrast. Considering that the fused images summarize the effective information in contact sensing, we will evaluate them in terms of information content and similarity. Information Entropy (IE) [26] is used to measure the amount of information contained in the fused image. Higher values represent richer information carried in the image and can reflect the effectiveness of the fusion operation. Meanwhile, the Multi-Scale Structural Similarity Index (MS-SSIM) [27] is used to evaluate the reliability of the fusion, which is obtained by the calculation of the fused image and the image captured using the camera. MS-SSIM values closer to one signify higher structural similarity, indicating that the fusion retains the information in the image to a higher extent. The images undergoing evaluation are normalized for gray values to unify the mapping relationships.

In Fig. 7, Table I and Table II, the evaluation results are displayed. Compared with the method of stitching based on motion distance sampling, the fused image obtained by our proposed method achieves higher metrics in the experiments. The image obtained by the method of stitching based on motion distance sampling is derived from the original image sequence without any modification of pixel values, and the image sequence itself has the same imaging conditions. The image obtained by our method in this case has slightly higher MS-SSIM values and significantly higher IE values. It indicates that our method can extract and enhance more image features without altering the integrity and reliability of the original information. The experiments have also shown that the number of images involved in fusion has an inconsistent correlation with the results in different scenes. Therefore, the number of samples required for performing fusion depends on the scene in the actual task.

## C. Application Demonstration

We also show the application of the proposed method in scene items. Fig. 8 shows the acquisition on a paper clip and a screw head. The fused image can present a larger area and more details of the object than the single image acquired by the sensor. However, it is worth noting that the sensor's

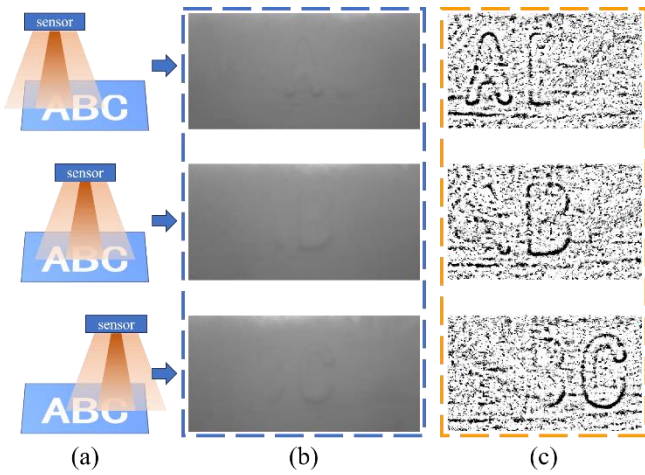


**Fig. 5.** Image sequence. (a) Demonstration of image acquisition. (b) Original image undergoing fusion. (c) Aligned image after binarization.

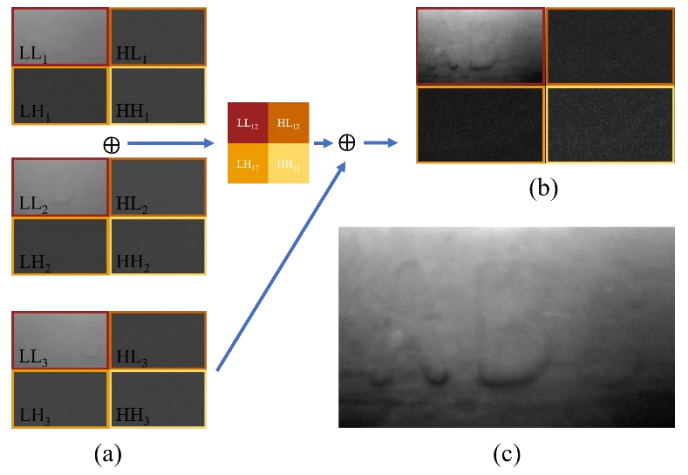


**Fig. 6.** Image fusion. (a) Wavelet transform and fusion process. (b) Fusion results. (c) Image after performing wavelet inversion.

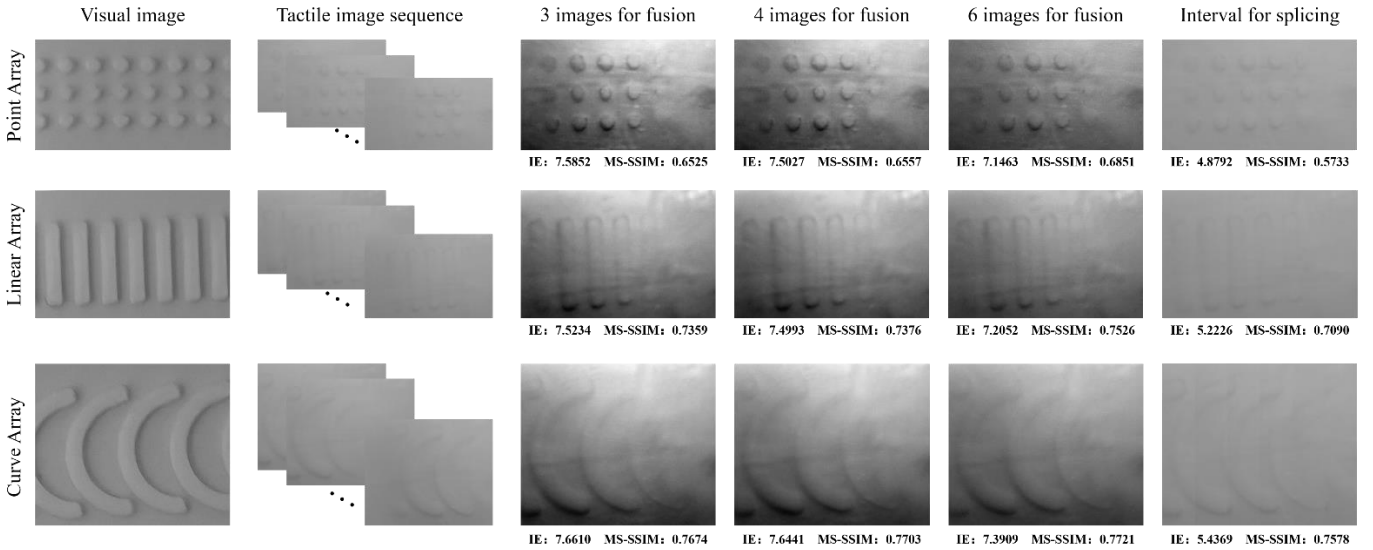


**Fig. 7.** Test results in the graphic matrices. Shows visual images captured by the camera, original image sequence, different numbers of fusion results and the splicing performed using uniformly selected regions. Each result shows the values of Information entropy (IE) and Multi-Scale Structural Similarity Index (MS-SSIM)

**TABLE I**  
THE EVALUATION RESULTS FOR IE

	3 images for fusion	4 images for fusion	6 images for fusion	Interval for splicing
point	7.5852	7.5027	7.1463	4.8792
line	7.5234	7.4993	7.2052	5.2226
curve	7.6610	7.6441	7.3909	5.4369

**TABLE II**  
THE EVALUATION RESULTS FOR MS-SSIM

	3 images for fusion	4 images for fusion	6 images for fusion	Interval for splicing
point	0.6525	0.6557	0.6851	0.5733
line	0.7359	0.7376	0.7526	0.7090
curve	0.7674	0.7703	0.7721	0.7578

capability to obtain morphological information effectively is limited for areas with depths beyond the reach of the sensor's flexible contact layer. For example, the texture deeper in the middle region of the screw head cannot be captured. In the meantime, we look forward to the application in acquiring fabric defects. The presence of defects in fabrics affects the price [28] and quality, so it is valuable to perform the detection.

Fig. 9 shows the effect of capturing defects in different types of fabrics. Compared to direct photographs of defects captured using a camera, a single contact image acquired by the sensor during contact can only capture a fraction of the fabric defect's features. The fused image combines the defect morphology features contained in the sequence of tactile images and can present more comprehensive and detailed information about the absence.

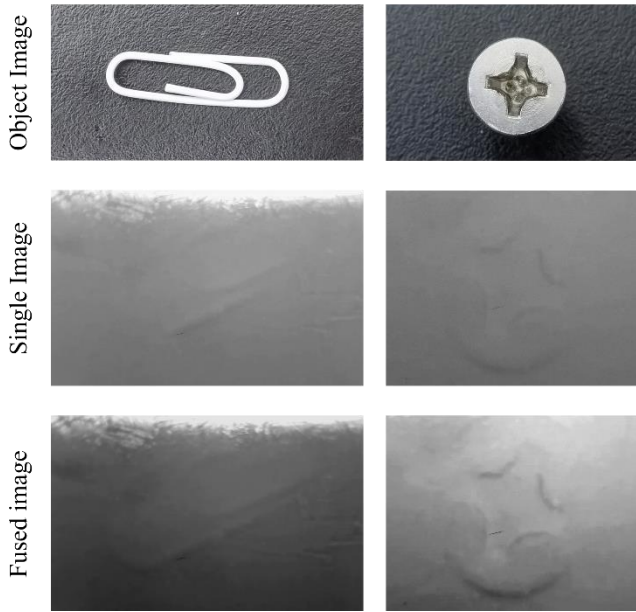


Fig. 8. Image fusion on everyday objects (paper clips, screws).

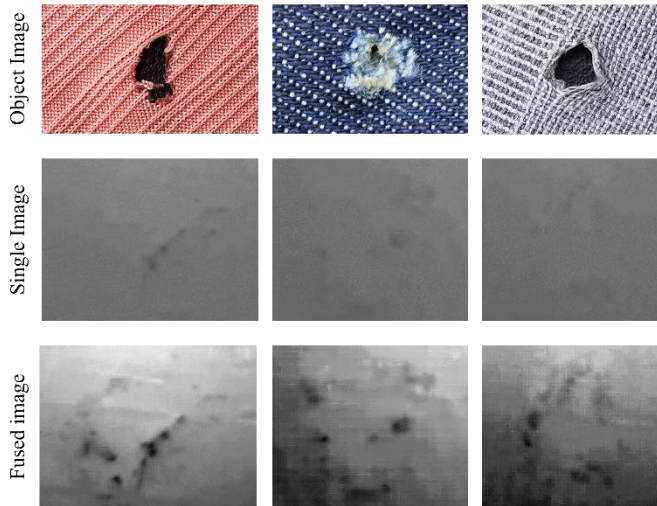


Fig. 9. Image fusion on defects of three fabrics.

#### IV. TACTILE IMAGES FOR TARGET DETECTION

We propose the method of fusing images to integrate the valid information in a sequence of images captured by cylindrical vision-based tactile sensors and simultaneously presenting the information at the deepest part of the contact on the image. An essential prerequisite for our fusion method is accurately aligning the features within the image, which requires finding the location of the features accurately. In addition, images acquired by tactile means also have many needs for performing target inspection and analysis in practical tasks. This means that it is necessary and promising to explore the capabilities of image sequences acquired by cylindrical vision-based tactile sensors in the task of target detection. In the experiments, it can be learned that although different contact depths in a single image will show different details, the basic features of the object can be recorded. This demonstrates the feasibility of target detection through single

images. We demonstrate the effect of performing target detection of defects using a neural network [29][30] in fabrics.

##### A. Neural network and experimental design

The core of defective target detection revolves around identifying the distinctive features present within the defective target in an image and effectively distinguishing them from other regions. The non-planar contact structure introduces inconsistency in the representation of object features across the image, posing challenges for feature extraction. Our approach employs deep learning instead of traditional image processing algorithms, such as feature statistics [31]. In practical applications, inspection devices are employed for the efficient examination of diverse objects, making it beneficial to simultaneously differentiate between object classes and detect defects. Therefore, a CenterNet network [32] combining classification [33] and target detection [34] was developed. Within this network, we used ResNet [35][36] as the backbone network for feature extraction. Additional output branches are Fig. 11(a) shows that our experimental setup involved selecting eight fabric samples. To ensure a standardized approach to defect detection, we manually simulated the creation of three distinct defect types: hole, scratch, and hairball, as illustrated in Fig. 11(b). We captured tactile images of the fabric using vision-based tactile sensors and labeled the information. These labeled data were applied to the data augmentation strategy [37][38] and subsequently fed into the network for training, as presented in Fig. 12(a). We employed ResNet50, implementing transfer learning [39] with pre-trained weights.

##### B. Experimental results and application outlook

The weight with the lowest loss value of the validation set in 150 epochs is used for performance evaluation. Regarding defect detection performance, the experiment yielded a mAP value of 90.90% when the Score Threshold was set to 0.5. Fig. 12(b)(c) shows the PR curve and AP. For the classification task, the confusion matrix in Fig. 12(d) highlights a remarkable accuracy of 99.83%. The algorithm's predicted output is visually represented in Fig. 13(a)-(d). The algorithm overcomes the difficulty of inhomogeneous feature information in images and performs strongly in extracting texture features. Real-time detection is critical in practical applications, and the cylindrical sensor's design lends itself to dynamic and continuous detection. By continuously detecting 100 images and recording the time taken, an FPS of 47.214 is obtained.

We have confirmed that a single image obtained by a cylindrical vision-based tactile sensor exhibits a high discriminatory capacity for detecting defective targets and recognizing the associated object class. This suggests that the image sequence is reliable for single-image applications. At the same time, combined with our proposed fusion method, the vision-based tactile sensor can potentially accomplish data acquisition and analysis in detection tasks. There is a chance that the acquired data can be further extracted with valuable information according to the requirements. Thus complete

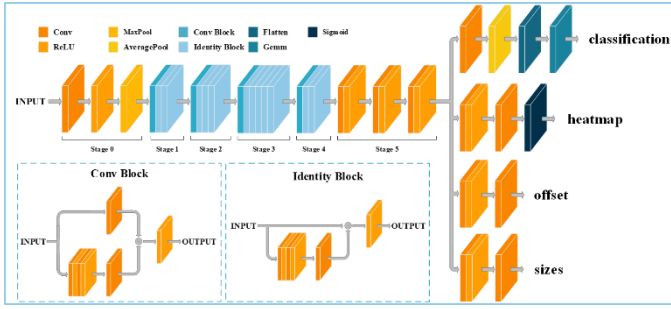


Fig. 10. Neural network structure.

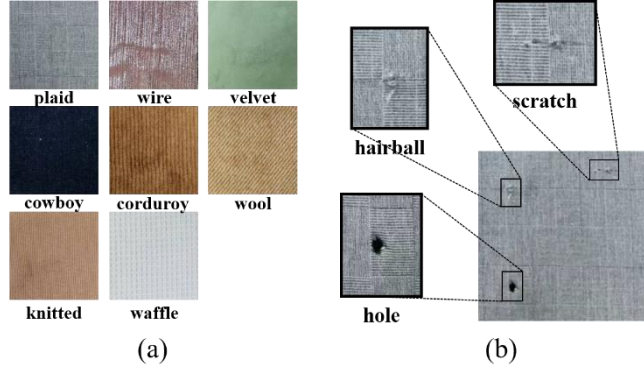


Fig. 11. Samples used to produce the dataset. (a) Eight fabrics. (b) Three defects.

object scanning and detection can be realized with only one sensor element and only one acquisition of the object, similar to multimodal sensing [40].

## V. CONCLUSION

In this work, we propose an image fusion method based on cylindrical vision-based tactile sensors. We employ a cylindrical structure's vision-based tactile sensor to capture a sequence of contact images, each containing information about varying contact depths. Based on the characteristics of contact depths, we extract information about different frequencies of the images in the frequency domain. The fusion is computed separately for high-frequency and low-frequency information. Experiments show that in object contact confronting an area larger than single sensing, the images fused with our proposed method have higher information and structural similarity compared with the method of stitching based on motion distance sampling. This means the effectiveness of our method and its usability in objects. At the same time, we explored the ability of a single image in an image sequence to perform target detection. Combined with CenterNet deep neural network, it shows high accuracy and application potential. This approach, which utilizes non-consistent contact depth, also has application potential in tactile sensors with conventional curved contact surfaces. Future improvements in our work include integrating the sensor hardware and the algorithm's robustness.

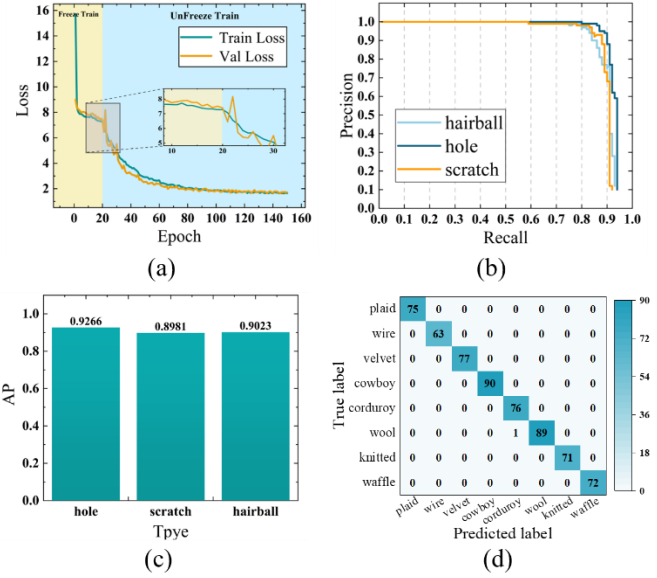


Fig. 12. (a) Loss value variation during the experimental training process. (b) PR curves for each type of defect detection target. (c) AP values of defect detection targets. (d) Confusion matrix for the category classification task.

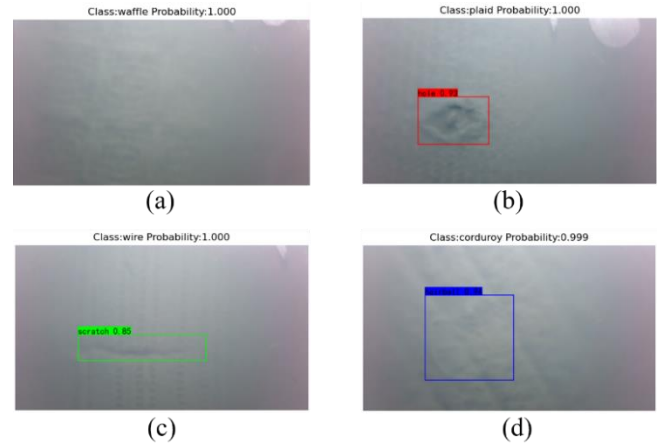


Fig. 13. (a) Predicted defect-free image and its category. (b)(c)(d) Shows the predicted three defective images and their categories.

## REFERENCES

- [1] Z. Lu and H. Yu, "GTac-Hand: A Robotic Hand With Integrated Tactile Sensing and Extrinsic Contact Sensing Capabilities," *IEEE/ASME Transactions on Mechatronics*, vol. 28, no. 5, pp. 2919-2929, Oct. 2023, doi: 10.1109/TMECH.2023.3264650.
- [2] B. L. Kodak and Y. Vardar, "FeelPen: A Haptic Stylus Displaying Multimodal Texture Feels on Touchscreens," *IEEE/ASME Transactions on Mechatronics*, vol. 28, no. 5, pp. 2930-2940, Oct. 2023, doi: 10.1109/TMECH.2023.3264787.
- [3] S. -H. Kim, U. Jeong and K. -J. Cho, "Multiparameter Remote Contact Force Sensor With Embedded Bend Sensing for Tendon-Driven Hand Robots," *IEEE/ASME Transactions on Mechatronics*, doi: 10.1109/TMECH.2023.3281062.
- [4] B. W. An, S. Heo, S. Ji, F. Bien and J. Park, "Transparent and flexible fingerprint sensor array with multiplexed detection of tactile pressure and skin temperature," *Nature Communications*, vol. 9, no. 2458, Jul. 2018, doi: 10.1038/s41467-018-04906-1.

- [5] Z. Zou, et al. "Monitoring Soft Shape Surface Deformation via Optical Images for the Distinction of Contact State," *Advanced Intelligent Systems*, 2023, doi: 10.1002/aisy.202300535.
- [6] B. Fang, Z. Xia, F. Sun, Y. Yang, H. Liu and C. Fang, "Soft Magnetic Fingertip With Particle-Jamming Structure for Tactile Perception and Grasping," *IEEE Transactions on Industrial Electronics*, vol. 70, no. 6, pp. 6027-6035, June 2023, doi: 10.1109/TIE.2022.3201305.
- [7] G. Kim, H. Chung and B. -K. Cho, "MOBINN: Stair-Climbing Mobile Robot With Novel Flexible Wheels," *IEEE Transactions on Industrial Electronics*, doi: 10.1109/TIE.2023.3319739.
- [8] W. Lin, B. Wang, G. Peng, Y. Shan, H. Hu and Z. Yang, "Skin-Inspired Piezoelectric Tactile Sensor Array with Crosstalk-Free Row+Column Electrodes for Spatiotemporally Distinguishing Diverse Stimuli," *Advanced Science*, vol. 8, no. 3, Feb. 2021, doi: 10.1002/adv.202002817.
- [9] Y. Lin and P. B. Shull, "Novel, Soft, Water-Filled Acoustic Waveguides for Simultaneous Tactile Force and Location Sensing," *IEEE Transactions on Industrial Electronics*, doi: 10.1109/TIE.2023.3308140.
- [10] S. Sundaram, P. Kellnhofer, Y. Li, J. Y. Zhu, A. Torralba and W. Matusik, "Learning the signatures of the human grasp using a scalable tactile glove," *Nature*, vol. 569, pp. 698-702, May. 2019, doi: 10.1038/s41586-019-1234-z.
- [11] G. H. Yang, W. Lee and S. Kang, "Development of Vibrotactile Pedestal With Multiple Actuators and Application of Haptic Illusions for Information Delivery," *IEEE Transactions on Industrial Informatics*, vol. 15, no. 1, pp. 591-598, Jan. 2019, doi: 10.1109/TII.2018.2850849.
- [12] K. Shimonomura, "Tactile Image Sensors Employing Camera: A Review," *Sensors*, vol. 19, no. 18, pp. 3933, Sep. 2019, doi: 10.3390/s19183933.
- [13] W. Xu, et al, "A Vision-Based Tactile Sensing System for Multimodal Contact Information Perception via Neural Network," 2023, arXiv:2310.01986
- [14] S. Cui, R. Wang, J. Hu, J. Wei, S. Wang and Z. Lou, "In-Hand Object Localization Using a Novel High-Resolution Visuotactile Sensor," *IEEE Transactions on Industrial Electronics*, vol. 69, no. 6, pp. 6015-6025, June 2022, doi: 10.1109/TIE.2021.3090697.
- [15] B. Ward-Cherrier et al, "The TacTip Family: Soft Optical Tactile Sensors with 3D-Printed Biomimetic Morphologies," *Soft Robotics*, vol. 5, no. 2, pp. 216-227, Apr. 2018, doi: 10.1089/soro.2017.0052.
- [16] R. Wattanapartint and K. Takemura, "Vision-based tactile sensing using multiple contact images generated by re-propagated frustrated total internal reflections," 2022 IEEE International Conference on Systems, Man, and Cybernetics (SMC), Prague, Czech Republic, 2022, pp. 962-967, doi: 10.1109/SMC53654.2022.9945094.
- [17] H. Sun, K. J. Kuchenbecker, G. Martius, "A soft thumb-sized vision-based sensor with accurate all-round force perception," *Nature Machine Intelligence*, vol. 4, pp. 135-145, Feb. 2022, doi: 10.1038/s42256-021-00439-3.
- [18] W. K. Do and M. Kennedy, "DenseTact: Optical Tactile Sensor for Dense Shape Reconstruction," 2022 International Conference on Robotics and Automation (ICRA), Philadelphia, PA, USA, 2022, pp. 6188-6194, doi: 10.1109/ICRA46639.2022.9811966.
- [19] G. Cao, J. Jiang, C. Lu, D. F. Gomes and S. Luo, "TouchRoller: A Rolling Optical Tactile Sensor for Rapid Assessment of Textures for Large Surface Areas," *Sensors*, vol. 23, no. 5, pp.2661, Feb. 2023, doi: 10.3390/s23052661.
- [20] B. Fang, X. Long, F. Sun, H. Liu, S. Zhang and C. Fang, "Tactile-Based Fabric Defect Detection Using Convolutional Neural Network With Attention Mechanism," *IEEE Transactions on Instrumentation and Measurement*, vol. 71, pp. 1-9, May. 2022, doi: 10.1109/TIM.2022.3165254.
- [21] K. Shimonomura, T. Chang and T. Murata, "Detection of Foreign Bodies in Soft Foods Employing Tactile Image Sensor," *Front Robot AI*, vol. 8, Dec. 2021, doi: 10.3389/frobt.2021.774080.
- [22] S. B. Campbell, Q. Wu, J. Yazbeck, C. Liu, S. Okhovatian, and M. Radisic, "Beyond Polydimethylsiloxane: Alternative Materials for Fabrication of Organ-on-a-Chip Devices and Microphysiological Systems," *ACS Biomaterials Science & Engineering*, vol. 7, no. 7, pp. 2880-2899, Aug. 2020, doi: 10.1021/acsbomaterials.0c00640.
- [23] J. Folkesson, H. Chang and N. Bore, "Lambert's Cosine Law and Sidescan Sonar Modeling," 2020 IEEE/OES Autonomous Underwater Vehicles Symposium (AUV), St. Johns, NL, Canada, 2020, pp. 1-6, doi: 10.1109/AUV50043.2020.9267946.
- [24] S. A. Cortez, L. Bokati, A. Velasco and V. Kreinovich, "Why Daubechies Wavelets Are so Successful," *Journal of Intelligent & Fuzzy Systems*, vol. 43, no. 6, pp. 6933-6938, Nov. 2022, doi: 10.3233/JIFS-212021.
- [25] Y. Ye, L. Bruzzone, J. Shan, F. Bovolo and Q. Zhu, "Fast and Robust Matching for Multimodal Remote Sensing Image Registration," *IEEE Transactions on Geoscience and Remote Sensing*, vol. 57, no. 11, pp. 9059-9070, Nov. 2019, doi: 10.1109/TGRS.2019.2924684.
- [26] W. Xu, Y. Pan, X. Chen, W. Ding and Y. Qian, "A Novel Dynamic Fusion Approach Using Information Entropy for Interval-Valued Ordered Datasets," *IEEE Transactions on Big Data*, vol. 9, no. 3, pp. 845-859, 1 June 2023, doi: 10.1109/TBDATA.2022.3215494.
- [27] I. Bakurov, M. Buzzelli, R. Schettini, M. Castelli and L. Vanneschi, "Structural similarity index (SSIM) revisited: A data-driven approach", *Expert Systems with Applications*, vol. 189, Mar. 2022, doi: 10.1016/j.eswa.2021.116087.
- [28] A. Kumar, "Computer-Vision-Based Fabric Defect Detection: A Survey," *IEEE Transactions on Industrial Electronics*, vol. 55, no. 1, pp. 348-363, Jan. 2008, doi: 10.1109/TIE.1930.896476.
- [29] Y. Huang et al., "4-DOF Visual Servoing of a Robotic Flexible Endoscope With a Predefined-Time Convergent and Noise-Immune Adaptive Neural Network," *IEEE/ASME Transactions on Mechatronics*, doi: 10.1109/TMECH.2023.3286850.
- [30] Z. Ding, W. Song, J. Xu, W. Cheng and S. Zhan, "A Deep-Learning-Based Low-Cost Micro-Leakage Measurement System for Industrial Applications," *IEEE/ASME Transactions on Mechatronics*, doi: 10.1109/TMECH.2023.3272797.
- [31] A. Abouelela, H. M. Abbas, H. Eldeeb, A. A. Wahdan, S. M. Nassar, "Automated vision system for localizing structural defects in textile fabrics," *Pattern Recognition Letters*, vol. 26, no. 10, pp. 1435-1443, Jul. 2005, doi: 10.1016/j.patrec.2004.11.016.
- [32] X. Zhou, D. Wang and P. Krähenbühl, "Objects as Points," Apr. 2019. [Online]. Available: arXiv: Computer Vision and Pattern Recognition, doi: 10.48550/arXiv.1904.07850.
- [33] S. Minaee, N. Kalchbrenner, E. Cambria, N. Nikzad, M. Chenaghlu and J. Gao, "Deep Learning--based Text Classification: A Comprehensive Review," *ACM Computing Surveys*, vol. 54, no. 3, pp. 1-40, Apr. 2021, doi: 10.1145/3439726.
- [34] Z. Zou, K. Chen, Z. Shi, Y. Guo and J. Ye, "Object Detection in 20 Years: A Survey," in *Proceedings of the IEEE*, vol. 111, no. 3, pp. 257-276, March 2023, doi: 10.1109/JPROC.2023.3238524.
- [35] K. He, X. Zhang, S. Ren and J. Sun, "Deep Residual Learning for Image Recognition," 2016 IEEE Conference on Computer Vision and Pattern Recognition (CVPR), Las Vegas, NV, USA, 2016, pp. 770-778, doi: 10.1109/CVPR.2016.90.
- [36] S. Yu, D. -H. Zhai and Y. Xia, "CGNet: Robotic Grasp Detection in Heavily Cluttered Scenes," *IEEE/ASME Transactions on Mechatronics*, vol. 28, no. 2, pp. 884-894, April 2023, doi: 10.1109/TMECH.2022.3209488.
- [37] J. Liu and Y. Ren, "A General Transfer Framework Based on Industrial Process Fault Diagnosis Under Small Samples," *IEEE Transactions on Industrial Informatics*, vol. 17, no. 9, pp. 6073-6083, Sept. 2021, doi: 10.1109/TII.2020.3036159.
- [38] A. Bochkovskiy, C. Wang, H. Liao, "YOLOv4: Optimal Speed and Accuracy of Object Detection," Apr. 2020. [Online]. Available: arXiv: Computer Vision and Pattern Recognition, doi: 10.48550/arXiv.2004.10934.
- [39] F. Zhuang et al., "A Comprehensive Survey on Transfer Learning," in *Proceedings of the IEEE*, vol. 109, no. 1, pp. 43-76, Jan. 2021, doi: 10.1109/JPROC.2020.3004555.
- [40] S. Shimadera, K. Kitagawa, K. Sagehashi, Y. Miyajima, T. Niiyama and S. Sunada, "Speckle-based high-resolution multimodal soft sensing," *Scientific Reports*, vol. 12, no. 13096, Jul. 2022, doi: 10.1038/s41598-022-17026-0.



**Zilan Li.** He has received the B.S. degree in South China Normal University, Guangzhou, China, in 2023. He is currently occupied in his M.S. degree in South China Normal University, Guangzhou, China. His currently interests include Optoelectronic intelligent sensing and deep learning.



**Zhibin Zou.** He has received the B.S. degree in Huaqiao University, Xiamen, China. He is currently occupied in his M.S.

degree in South China Normal University, Guangzhou, China. His currently interests include optoelectronic technology and intelligent sensing.



sensing design.

**Weiliang Xu** received B.S. degree in South China Normal University, Guangzhou, China, in 2022. He is currently occupied in his Ph.D. degree in South China Normal University, Guangzhou, China. His current interests include Human-Computer Interaction and optoelectronic intelligent



intelligent system design.

**Yuanzhi Zhou**. He was received B.S. degree in School of Physics, Hefei University of Technology, Hefei, China. He is currently occupied in his Ph.D. degree in South China Normal University, Guangzhou, China. His current interests include Human-Computer Interaction and



**Guoyuan Zhou** received the bachelor's degree in Optical Information Science Engineering from Nanjing Tech University. He is currently occupied Ph.D. in South China Normal University. His current interests include vision-based tactile sensors.



and intelligent sensing design.

**Xuan Huang**. She received her B.S. degree from Yanshan University in Qinhuangdao, Hebei, China in 2021. She is currently pursuing a M.S. degree in the South China Normal University in Guangzhou, Guangdong Province, China. Her current interests include flexible ionic electronics



and intelligent sensing design.

**Xinming Li** received his B.Sc. and Ph.D. degrees from Tsinghua University in 2007 and 2013, respectively. After that, he was an Assistant Professor at the National Center for Nanoscience and Technology, China, postdoctoral research fellow at The Chinese University of Hong Kong, research fellow at The Hong Kong Polytechnic University, and JSPS postdoctoral Fellow at the National Institute for Materials Science, Japan. He is currently a Professor with the School of Information and Optoelectronic Science and Engineering, at South China Normal University, China. He has co-authored more than 90 journal publications. His research interests include wearable devices, optoelectronic technology, vision-based tactile sensors, intelligent sensing systems, and haptics technology. He served as editor for *Sensors*, and *Frontiers in Physics*.